

Platelet margination dynamics in blood flow: The role of lift forces and red blood cells aggregation

Mariam Dynar^{1,*}, Hamid Ez-Zahraouy,² Chaouqi Misbah^{1,†} and Mehdi Abbasi^{1,3,‡}

¹*Université Grenoble Alpes, CNRS, LIPhy, F-38000 Grenoble, France*

²*Laboratoire de Matière Condensée et Sciences Interdisciplinaires, URL-CNRST,
Mohammed V University in Rabat, Rabat, Morocco*

³*Aix Marseille Univ, CNRS, CINAM, Turing Centre for Living Systems, Marseille, France*



(Received 15 November 2023; accepted 12 July 2024; published 13 August 2024)

Homeostasis plays a critical role in maintaining the delicate balance between preventing excessive bleeding and enabling clot formation during injuries. One pivotal aspect of homeostasis involves the development of platelet clots. In this study, we analyze numerically the behavior of platelet margination as a function of the adhesion energy between red blood cells (RBCs), driven by the presence of plasma proteins. We examine scenarios encompassing both physiological conditions and pathological states, such as those seen in patients with diabetes. Employing a two-dimensional simulation, we utilize rigid particles and a vesicle model to simulate platelets and RBCs, respectively. We employ the lattice Boltzmann method to solve the underlying model equations. We first demonstrate that platelet margination is primarily determined by lift forces and is not notably affected by whether the cells undergo tank-treading (TT) or tumbling (TB) behavior, as often reported. Specifically, we unveil instances where cells exhibit TT or TB behavior, yet their platelet concentration profiles closely resemble each other. Furthermore, we present a striking result concerning the impact of RBC adhesion. In microcirculation the hematocrit is in the range 5–20%. A moderate adhesion energy (falling within the physiological range) boosts platelet margination in microcirculation. However, this effect becomes small for larger hematocrit encountered in macrocirculation (e.g., 40%). This boost is more significant for a viscosity contrast (viscosity of cytoplasm over that the suspending fluid) equal to a known value for RBCs, as compared to the case without viscosity contrast. As we increase the adhesion energy (the pathological range), a noteworthy decline in platelet margination is found, albeit that for some flow strength the platelet margination reaches a minimum and increases again at higher adhesion energy. These results can be attributed to a combination of lift generated by the bounding walls and the formation of RBC clusters. Notably, our study sheds light on a critical consequence of excessive adhesion, typically observed in pathological conditions like diabetes mellitus.

DOI: [10.1103/PhysRevFluids.9.083603](https://doi.org/10.1103/PhysRevFluids.9.083603)

I. INTRODUCTION

Red blood cells (RBCs) are essential for the delivery of oxygen and nutrients to tissues and organs. RBCs are the predominant blood cells; they occupy about 45% of the total blood volume,

*Contact author: mariam.dynar@univ-grenoble-alpes.fr

†Contact author: chaouqi.misbah@univ-grenoble-alpes.fr

‡Contact author: mehdi1abbasi@gmail.com

while plasma occupies about 55% and other cells (platelets, white cells) less than 1%. The permanent mutual interaction between RBCs and vessel walls as well as among RBCs dictates the overall blood flow properties. Platelets—thrombocytes—are the smallest blood cells in the human body. Their number is approximately 1.5×10^{11} platelets per liter, and their diameter is between 2 and $4 \mu\text{m}$ (significantly smaller than RBC diameter, which is about $8 \mu\text{m}$) [1]. The main functions of platelets are to recognize and repair damaged endothelium (the monolayer of endothelial cells lining the internal surface of blood vessels) [2]. This monolayer of cells is responsible for the control of vascular permeability and intervenes in immune responses at places of infection or injury [3]. Another important role of platelets is to activate the process of blood clotting to stop bleeding [4]. More precisely, blood clotting in this process consists of a platelet-plug formation, and is the most important step in homeostasis (the process of stopping bleeding due to an injury).

An important question, regarding platelets, which has been thoroughly addressed in the literature pertains to their margination by RBCs: RBCs have a tendency to push platelets toward the vessel periphery [5–7]. If this is the case *in vivo*, this effect would mean that platelets are often located close to vessel walls and ready to initiate homeostasis in case of an injury, or to contribute, via a complex pathway, to repairing damaged endothelium.

Before describing the main focus of the present work, let us first recall the main results regarding margination of platelets. Under physiological conditions, platelets tend to move toward vessel walls; this phenomenon is called platelet margination [6]. It is known that the platelet's margination rate is affected by the shape and the size of platelets [5,6]. Unactivated platelets can be considered rigid discoidal particles. Activated platelets change their shape from a discoid shape to a spherical shape. This shape change is caused by the contact between platelets and endothelial cells or by their exposure to circulating agonists [8]. According to *in vitro* study, platelet margination is caused by the hydrodynamic interaction between RBCs and platelets [5,7]. Moreover, RBC properties may impact the platelet margination. In a numerical study, Reasor *et al.* [6] modeled RBC and platelet flow in three dimensions using the lattice Boltzmann method (LBM) and found that the increase of RBC deformability as well as the increase of the hematocrit enhance platelet margination. They also reported that the inner viscosity of RBCs affects inversely the platelet margination [6]. Furthermore, it has been shown that there exists an optimal wall shear rate value corresponding to the maximum of the platelet's margination rate [4,9]. Moreover, it has been reported that this critical shear rate value depends on the tube diameter [4]. Besides platelet margination, margination of white blood cells [10–13] as well as that of rigid RBCs have also been studied [14].

Many studies of platelet margination by RBCs have been based on numerical simulations [4–6,9,15–20] or on *in vitro* experimental studies [7,21–24], and focused on physiologically inspired situations. There are, however, several pathological situations which have not been yet addressed. One typical example is the case where RBCs form more or less robust aggregates. Under physiological conditions, aggregates are reversible; that is, they form and they dissociate in the course of time. There are pathological situations where aggregates can form in an irreversible way. It is known, for example, that patients suffering from diabetes can have robust aggregates that may even lead to blood occlusions in microcirculation [25]. Our aim here is to analyze platelet margination in the presence of RBC aggregates. Fibrinogen is believed to be the main protein responsible for RBC aggregate formation. It is often reported that fibrinogen within diabetic patients has higher concentrations ($6.56 \pm 1.30 \text{ mg/ml}$) than normal range ($3.24 \pm 1.39 \text{ mg/ml}$) [26], a fact that can enhance aggregation.

In the present work, we analyze systematically the platelet margination process by means of two-dimensional (2D) simulation in the presence of RBC aggregation. Our simulations consists of a confined binary suspension of rigid particles and deformable 2D particles (vesicles, a widely adopted simple model for RBCs) mimicking platelet and RBCs, respectively. We find that, when the adhesion force between RBCs is not too strong, the platelet margination is boosted for hematocrits relevant to microcirculation (lying in the range 5–20% [27–30]). However, for higher hematocrits the effect is less pronounced. For a high enough adhesion energy (mimicking pathological situations), the RBCs tend to form stable aggregates. This leads to a reduction of platelet margination,

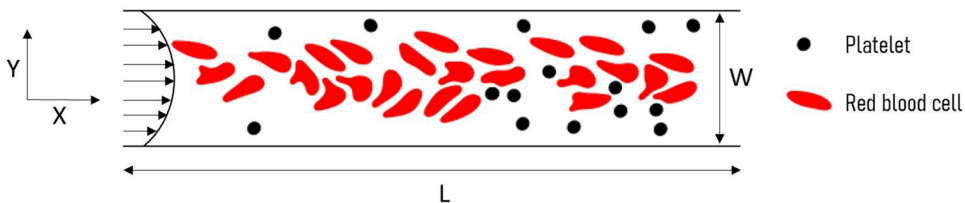


FIG. 1. Binary suspensions of RBCs and platelets under parabolic flow.

but for some flow strengths we observe a second increase of margination at high adhesion energies. In order to dig further into the link between adhesion force and platelet margination, we explore the behavior of a cell free layer as a function of the adhesion energy between RBCs and we find that the cell free layer thickness decreases upon increasing the adhesion energy between RBCs. Finally, we analyze the role of viscosity contrast. When the viscosity contrast is high enough, we find a decrease in the margination. Contrary to previous claims [4,6], it is not the decrease of tank treading of the membrane (which is reduced upon increasing the viscosity contrast) which reduces directly the margination, but it is rather an indirect effect: the transverse migration (or lift) of RBCs is reduced due to an increase of viscosity contrast, and this leads, in turn, to a decline of the margination effect.

II. METHODOLOGY

Two-dimensional simulations are performed to carry out our study. The simulation is based on the LBM. The 2D model was selected for computational efficiency. In 2D simulation, the membrane is considered a contour instead of a surface. It has been reported that the 2D model captures many shapes and phenomena observed in three dimensions. Indeed, the parachute and slipper shapes [31,32] and the multilobe shape [33–35] are observed both in two and three dimensions. In addition, the shapes of aggregated RBC doublets at equilibrium [36] share strong similarity between 2D and three-dimensional (3D) models. In addition, the phase diagram (in the plane of flow strength and adhesion energy) of the aggregates (a topic of the present study) obtained in two dimensions is quite similar to that found in three dimensions [37].

RBCs and platelets are modeled here by 2D vesicles and rigid particles, respectively. A suspension of vesicles and rigid particles is set in a straight channel of length L and width W . A long enough tube is needed to simulate the process of margination (a tube length of about $330\ \mu\text{m}$ was necessary), due to the length and timescales necessary for the margination process to show up in a significant manner [6]. The suspension is subjected to a Poiseuille flow, by applying a body force in the LBM, briefly recalled below. The schematic of the system is illustrated in Fig. 1.

The imposed velocity (in the absence of cells) along x and y axes reads

$$U_x = \frac{4U_{\max}}{W^2}(Wy - y^2), \quad U_y = 0, \quad (1)$$

where U_{\max} is the maximum velocity, which is attained at the center line located at $y = \frac{W}{2}$. The total flow field (the imposed one and that induced by the presence of the cells) of internal and external fluids obeys the Navier-Stokes (NS) equations:

$$\rho \left(\frac{\partial \mathbf{u}}{\partial t} + \mathbf{u} \cdot \nabla \mathbf{u} \right) = -\nabla p + \eta \nabla^2 \mathbf{u} + \mathbf{f}, \quad (2)$$

$$\nabla \cdot \mathbf{u} = 0, \quad (3)$$

where ρ , \mathbf{u} , and p are respectively the density, velocity, and pressure. η is the viscosity of the fluid, where $\eta = \eta_{\text{in}}$ will denote the viscosity of the fluid inside the vesicles and $\eta = \eta_{\text{ex}}$ that of suspending fluid. \mathbf{f} is the force applied by the vesicle on the fluid, to be specified below.

The membrane energy contains three contributions: the bending energy, the membrane incompressibility condition [38], and the adhesion energy between all vesicles (which will be modeled by a Lennard-Jones potential). The cell membrane is indicated by Γ . In two dimensions, the energy of the membrane is given by

$$E = \sum_i E_i^b + \sum_{i \neq j} E_{i,j}^{\text{adh}}, \quad (4)$$

where

$$E_i^b = \frac{k}{2} \oint_{\Gamma_i} c^2 ds + \oint_{\Gamma_i} \zeta ds \quad (5)$$

is both the bending and incompressibility energy of the i th vesicle, and

$$E_{i,j}^{\text{adh}} = \varepsilon_0 \oint_{\Gamma_i} ds(\mathbf{m}_i) \oint_{\Gamma_j} ds(\mathbf{m}_j) \phi(|\mathbf{m}_i - \mathbf{m}_j|) \quad (6)$$

is the adhesion energy between the i th and j th vesicles. ds corresponds to the distance between two adjacent membrane points, c and k are respectively the local curvature of the membrane and the membrane bending rigidity (taken to be $k = 4 \times 10^{-19}$ J), ζ is a local Lagrange multiplier associated with the constraint of local perimeter inextensibility, and $\phi = -2\left(\frac{h}{r_{ij}}\right)^6 + \left(\frac{h}{r_{ij}}\right)^{12}$ is the Lennard-Jones potential which describes attractive interaction at long ranges and repulsive interaction at short ranges. h is the equilibrium distance between two different points located on two different vesicles i and j . In the literature [39], it has been reported that the intercellular distance is about 25 nm for RBCs in plasma. In our simulation, due to a compromise between computational time and spatial resolution, we have set $h = 400$ nm. The chosen distance ensures a good agreement between simulation and experiments, as reported in previous studies [36,40,41]. ε_0 is the minimum energy associated to this distance. $\mathbf{r}_{ij} = \mathbf{m}_i - \mathbf{m}_j$ is the vector between two points sitting on two different vesicle membranes, where \mathbf{m}_i and \mathbf{m}_j are the two position vectors of the two points of the i th and j th vesicles.

Before proceeding further, a remark is in order. Neu and Meiselman [42] proposed initially a quite involved model for interaction energy between RBCs. Their model was successfully confronted with experimental data [43]. It has also been shown that the Neu-Meiselman model can be well approximated by a Morse potential [44], which is well approximated by a Lennard-Jones potential [45]. Other experimental data based on atomic force microscopy measurement seem consistent with a Lennard-Jones-like potential [46], albeit no systematic attempt was made there.

The membrane force can be obtained by the functional derivative of the energy [Eq. (4)]. The total membrane force is expressed as

$$\mathbf{F}(\mathbf{m}_i) = \mathbf{F}^b(\mathbf{m}_i) + \mathbf{F}^{\text{adh}}(\mathbf{m}_i), \quad (7)$$

where

$$\mathbf{F}^b(\mathbf{m}_i) = k \left[\frac{\partial^2 c}{\partial s^2} + \frac{c^3}{2} \right] \mathbf{n} - c \zeta \mathbf{n} + \frac{\partial \zeta}{\partial s} \mathbf{t} \quad (8)$$

is the functional derivative of the bending energy supplemented with the membrane incompressibility condition, and \mathbf{n} and \mathbf{t} are respectively the normal and tangential unit vectors. More details can be found in Ref. [47].

The adhesion force takes the form

$$\mathbf{F}^{\text{adh}}(\mathbf{m}_i) = -\varepsilon_0 \sum_{j \neq i} \int_{\Gamma_j} \left[\frac{d\phi(r_{ij})}{dr_{ij}} \left(\frac{\mathbf{r}_{ij}}{r_{ij}} \cdot \mathbf{n}(\mathbf{m}_i) \right) + c(\mathbf{m}_i) \phi(r_{ij}) \right] \mathbf{n}(\mathbf{m}_i) ds(\mathbf{m}_j), \quad (9)$$

obtained by the functional derivative of the adhesion energy between i th and j th vesicles.

The dimensionless form of the forces can be written as

$$\bar{\mathbf{F}}^b(\mathbf{m}_i) = \left[\frac{\partial^2 \bar{c}}{\partial \bar{s}^2} + \frac{\bar{c}^3}{2} \right] \mathbf{n} - \bar{c} \bar{\zeta} \mathbf{n} + \frac{\partial \bar{\zeta}}{\partial \bar{s}} \mathbf{t} \quad (10)$$

and

$$\bar{\mathbf{F}}^{\text{adh}}(\mathbf{m}_i) = -\bar{\varepsilon}_0 \sum_{j \neq i} \int_{\Gamma_j} \left[\frac{d\bar{\phi}(\bar{r}_{ij})}{d\bar{r}_{ij}} \left(\frac{\bar{\mathbf{r}}_{ij}}{\bar{r}_{ij}} \cdot \mathbf{n}(\mathbf{m}_i) \right) + \bar{c}(\mathbf{m}_i) \bar{\phi}(\bar{r}_{ij}) \right] \mathbf{n}(\mathbf{m}_i) d\bar{s}(\mathbf{m}_j). \quad (11)$$

The dimensionless variables are defined as follows:

$$\bar{F} = \frac{R_0^3 F}{k}, \quad \bar{\varepsilon}_0 = \frac{R_0^3 \varepsilon_0}{k}, \quad \bar{c} = cR_0, \quad \bar{s} = \frac{s}{R_0}, \quad \bar{r}_{ij} = \frac{r_{ij}}{R_0}, \quad \bar{\phi}(\bar{r}_{ij}) = \phi(\bar{r}_{ij}R_0). \quad (12)$$

Let us recall that ε_0 is the minimal energy between two points belonging to two different vesicles. In fact, the adhesion energy between two planes (like when two vesicles adhere to each other with a straight shape in the adhered region), the minimal energy is different from ε_0 , denoted as ε , and is equal to [37]

$$\varepsilon = 1.6862h\varepsilon_0. \quad (13)$$

In the spirit of the LBM, the force acting on the membrane is treated in an immersed sense *à la* Peskin [48]. The force action is defined in the 2D domain (not only at the membrane). For any given point of coordinate \mathbf{r} of the fluid domain we define the force as

$$\mathbf{f}(\mathbf{r}) = \int_{\Gamma} \mathbf{F}(\mathbf{m}_i) \delta^{2D}(\mathbf{r} - \mathbf{m}_i) ds \quad (14)$$

Where δ^{2D} is the 2D smeared Dirac function. More details about the mathematical model can be found in Ref. [49].

A. Lattice-Boltzmann method

Fluid flow simulation is performed using the lattice Boltzmann method. In LBM, the fluid is considered a set of pseudofluid particles, which can collide with each other and propagate. The spatial position and the velocity of pseudoparticles are discretized. This means that every pseudoparticle is allowed to move just along specific directions with given discrete speeds.

A distribution function $f_i(\mathbf{r}, t)$ is associated with each single pseudofluid particle. $f_i(\mathbf{r}, t)$ gives the probability of finding the pseudofluid particle at time t , at position \mathbf{r} (the discrete lattice nodes position vector) having velocity c_i in the i direction. The time evolution of $f_i(\mathbf{r}, t)$ is governed by the Boltzmann equation [composed of streaming operation (left) and collision operation (right)], expressed as

$$f_i(\mathbf{r} + \mathbf{c}_i, t + 1) - f_i(\mathbf{r}, t) = -\frac{1}{\tau} [f_i(\mathbf{r}, t) - f_i^{(0)}(\mathbf{r}, t)], \quad (15)$$

where τ is the relaxation time and $f_i^{(0)}(\mathbf{r}, t)$ is the equilibrium distribution obtained from an approximation of the Maxwell-Boltzmann distribution. In this study, we use the D2Q9 lattice, where D2 stands for two-dimensional space and Q9 represents the total number of discrete allowed velocity vectors. The hydrodynamical macroscopic quantities describing the flow are given by (i) the local mass density $\rho(\mathbf{r}, t) = \sum_{i=0}^8 f_i(\mathbf{r}, t)$, (ii) the local fluid velocity $\mathbf{u}(\mathbf{r}, t) = \frac{1}{\rho(\mathbf{r}, t)} \sum_{i=0}^8 f_i(\mathbf{r}, t) \mathbf{c}_i$, and (iii) the local fluid pressure $p(\mathbf{r}, t) = \rho(\mathbf{r}, t) c_s^2$ ($c_s = 1/\sqrt{3}$ is the lattice speed of sound). In order to impose a Poiseuille flow, a constant term, F_i , representing a volumic force, is added on the right-hand side of Eq. (15). Further details on this issue, and in general on the LBM, can be found in Refs. [50–52].

B. Dimensionless parameters

Several dimensionless parameters enter our problem (dimensionless parameters are calculated relative to RBC dimensions and characteristics).

(i) The Reynolds number is given by

$$\text{Re} = \frac{\rho \dot{\gamma} R_0^2}{\eta_{\text{ex}}}. \quad (16)$$

(ii) The capillary number, which quantifies the flow strength over bending rigidity of the membrane (in our study, we maintained the capillary number within the range of 30 to 70, which corresponds to shear rate values ranging from 550 to 1000 s^{-1} measured in the arterioles), is given by

$$\text{Ca} = \frac{\eta_{\text{ex}} \dot{\gamma} R_0^3}{k} = \tau_c \dot{\gamma}, \quad (17)$$

where $\tau_c = \eta_{\text{ex}} R_0^3 / k$ is the shape relaxation time of the vesicle.

(iii) The confinement, which describes the ratio between effective vesicle diameter and channel width, is given by

$$C_n = \frac{2R_0}{W}. \quad (18)$$

(iv) The viscosity contrast, which is the ratio between the viscosities of internal and external fluids (η_{in} and η_{ex} , respectively), is given by

$$\lambda = \frac{\eta_{\text{in}}}{\eta_{\text{ex}}}. \quad (19)$$

(v) The reduced area combines the vesicle perimeter P and its enclosed area A :

$$\tau = \frac{4A\pi}{P^2}, \quad (20)$$

where $\tau = 1$ for a circle and is less than unity for any other shape.

(vi) The hematocrit, which refers to the total area percentage of RBCs within the channel, is given by

$$\phi(\%) = \frac{nA}{WL} \times 100, \quad (21)$$

where n is the number of cells within the computation domain.

(vii) The dimensionless macroscopic adhesion energy is defined as

$$\bar{\varepsilon} = \frac{\varepsilon R_0^2}{k}, \quad (22)$$

where k is the bending rigidity of the membrane (taken to be $k = 4 \times 10^{-19}$ J), R_0 , taken to be $R_0 = 3 \mu\text{m}$, is the effective vesicle radius, $\dot{\gamma}$ is the applied shear rate, W is the channel width, and ε is the adhesion energy between two vesicles (directly related to the concentration of fibrinogen [40]). The interaction energy between two RBCs was quantified using single cell force microscopy at various fibrinogen and Dextran levels by Brust *et al.* [40]. Table I summarizes their results. From Table I, we can estimate which range of protein level corresponds to our simulation condition and whether our condition is physiological or pathological.

TABLE I. Fibrinogen concentration and the associated interaction energy and dimensionless macroscopic adhesion energy [40]. Physiological values are indicated with blue, pathological values with red, and the intermediate state with orange.

Fibrinogen concentration (mg/ml)	0.898	2.391	4.197	5.402	6.597	8.098
Interaction energy ($\mu\text{J}/\text{m}^2$)	1.884	2.719	3.748	4.655	4.922	-6.566
Dimensionless macroscopic adhesion energy, $\bar{\varepsilon}$	42.38	61.17	84.33	104.73	110.74	147.73

The LBM, using the immersed boundary method (IBM), was adopted to perform our 2D simulation [52,53]. The Reynolds number is set to $\text{Re} = 0.1$, which is a value that ensures a good balance between numerical efficiency and good precision for the Stokes regime [54]. The value of the reduced area is set to $\tau = 0.64$ for RBCs (this value provides a biconcave equilibrium shape and is inspired by that of human RBCs) and $\tau = 1$ for platelets (a circular shape). The confinement value was set to $C_n = 0.2$ during simulation. Table II presents the simulation parameters used in this article.

III. RESULTS

In this section we present the main results by analyzing the effects of the three main parameters: (i) capillary number, (ii) viscosity contrast, and (iii) adhesion energy.

A. The effect of the capillary number on platelet margination

The present section is dedicated to the examination of how the capillary number affects the platelet distribution near walls. For that purpose, we performed simulations of RBCs and platelets flowing through two channels of different confinements $C_n = 0.2, 0.4$ (corresponding channel widths $D = 15 \mu\text{m}, 30 \mu\text{m}$, respectively). Once the particles were prepared inside the channel, we applied a parabolic flow with different capillary numbers $\text{Ca} = 5, 30, 70$; these values are in the wall shear rate range of arterioles and venules.

Figure 2 presents the average time needed by half of the platelets to reach the cell free layer (CFL). Figure 2 shows that the increase of the capillary number from $\text{Ca} = 5$ to $\text{Ca} = 70$ in the case of $C_n = 0.2$ does not affect the margination. In contrast, for a confinement $C_n = 0.4$, platelets spend less time to reach the CFL. Moreover, increasing the capillary number, the platelets need less time to reach the CFL.

Figure 3 shows the local concentration averaged over time of platelets (ϕ_{plt}) and of RBCs (ϕ_{RBC}) in the channel. For confinement $C_n = 0.2$ [Fig. 3(a)], the increase of shear rate does not affect the margination. In contrast, when $C_n = 0.4$, margination becomes fast and strong when the capillary number varies from $\text{Ca} = 5$ to $\text{Ca} = 30$ [Fig. 3(b)]. In both cases $C_n = 0.2$ and $C_n = 0.4$, the concentration of platelets near the wall is roughly the same for $\text{Ca} = 30$ and $\text{Ca} = 70$, because $\text{Ca} = 30$ is sufficient to ensure the maximum of margination. These observations are in line with those of Krüger [4]. In that study, the dependency of the platelet's margination on the channel

TABLE II. Simulation parameters inspired by human RBCs.

Parameter	Physical unit
R_0	$3 \mu\text{m}$
η_{ex}	1 mPa s
k	$4 \times 10^{-19} \text{ J}$
τ_c	0.067 s

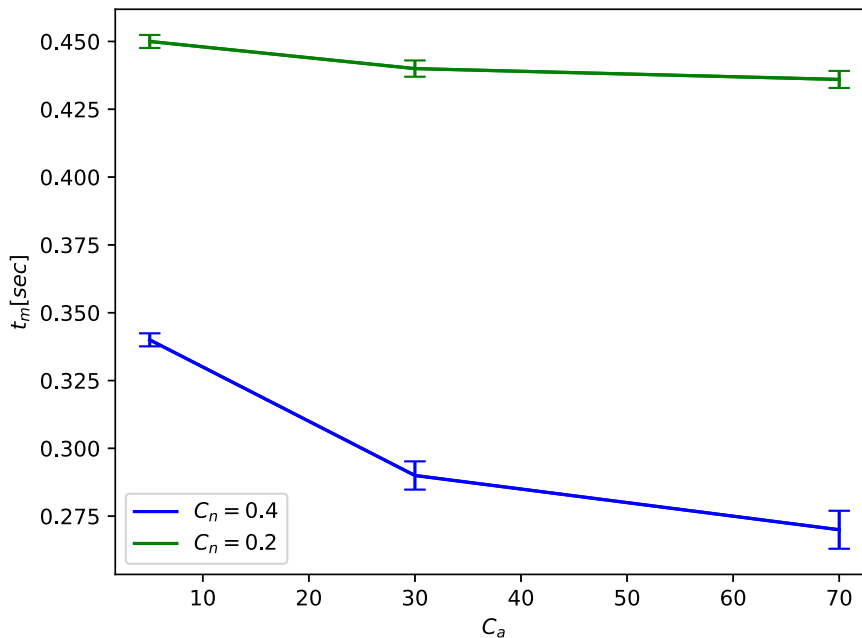


FIG. 2. The average time needed by half of the platelets to reach the cell free layer for $C_n = 0.2, 0.4$ as a function of C_a .

diameter and capillary number was studied, using three-dimensional simulations with deformable and nearly rigid particles mimicking RBCs and platelets, respectively. They figured out that the margination is fast for high capillary number with channel diameter up to $20 \mu\text{m}$. However, there is no strong difference in platelet margination in the case of channel diameter greater than $20 \mu\text{m}$. Our two-dimensional model of RBCs, which takes into account the RBC membrane properties without cytoskeleton, captures these features and constitutes an interesting test before embarking on the main question of this study.

B. The importance of wall lift on platelet margination

The aim of this section is to highlight the importance of the migration due to the walls (named lift) in the process of margination. Generally, the cross-streamline migration of RBCs can be due both to the presence of bounding walls as well as to the flow curvature [55]. The case of a vesicle in a semibounded channel was investigated by Kaoui *et al.* [47]. As a conclusion, they found that the lift due to the presence of the wall dominates over that due to flow curvature. A more systematic study by Nix *et al.* [56] showed that the wall lift force often dominates, except for high enough viscosity contrast ($\lambda = 5$), where the two forces become of comparable order, provided that the cell is far away from the wall (at a distance of about 20 times the radius); for smaller distances the wall lift dominates. Note also that far away from the center and, *a fortiori*, in the vicinity of the wall the flow field is rather linear, so that we expect the wall lift force to be the dominant factor in creating the CFL.

The results of this section will be useful in interpreting the effect of adhesion energy on the margination process. It is known that at low viscosity contrast value, vesicles under shear flow undergo tank-treading (TT) dynamics (the vesicle adopts a fixed orientation and the membrane rotates around the inner fluid in a tank-tread fashion), whereas at high enough value of viscosity contrast vesicles exhibit tumbling (TB) dynamics where the vesicle rotates as a rigid body [57,58]. The critical value of the viscosity contrast that corresponds to the transition between tank treading

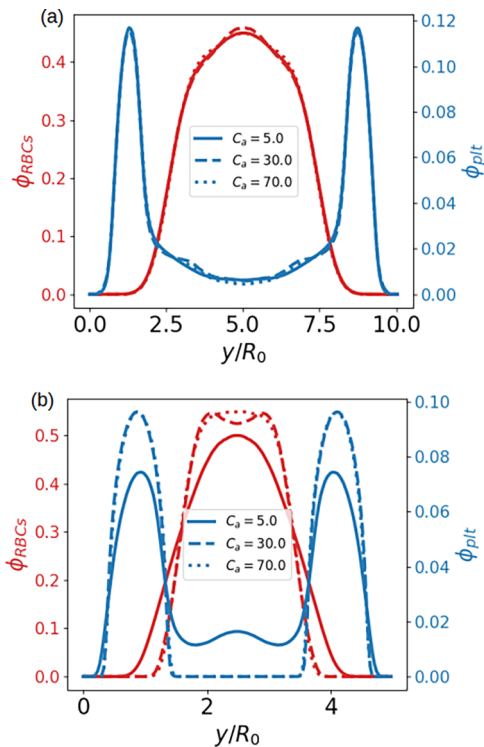


FIG. 3. Time-averaged concentration profile of platelets (ϕ_{plt}) and RBCs (ϕ_{RBC}) for $\text{Ca} = 5, 30, 70$, $\lambda = 1$, $C_n = 0.2$, $\phi = 0.20$, and $\bar{\varepsilon} = 0$. (a) $C_n = 0.2$; (b) $C_n = 0.4$. The dotted, dashed, and solid blue and red lines represent the time-averaged concentration profiles of platelets and RBCs, respectively. The dotted and dashed blue lines in (b) are superposed.

and tumbling depends on confinement and reduced area [59]. In the TT regime, and at low enough viscosity contrast, the angle made by the vesicle with the flow direction is large enough, so that there is a strong upstream-downstream asymmetry, leading to a large enough lift. When the viscosity contrast is close to the critical value for TT-TB transition, the vesicle orientation angle is close to zero, leading to a very small upstream-downstream asymmetry, and thus to a very small lift (owing to the Stokes reversibility upon time reversal). In the TB regime, on an average over a period of TB, there is upstream-downstream symmetry, and thus the lift is almost zero. Thus, the lift (migration due to wall) critically depends on the type of dynamics. Since lift is small in the TB regime, it is natural to expect a decline of platelet margination in this regime. Actually, Krüger [4] has found that in the TT regime the margination is significantly stronger than in the TB regime. It has also been reported that decreasing viscosity contrast enhances platelet margination [6]. Here we stress that the key point that influences margination is not TT or TB itself, but rather the evolution of the lift due to walls, as will be seen below.

We performed simulations by fixing the confinement and the capillary number to $C_n = 0.2$ and $\text{Ca} = 30$. We selected three values of viscosity contrasts, two for which a single vesicle undergoes TT ($\lambda = 1$ and $\lambda = 5$) and one value for which a single vesicle undergoes TB ($\lambda = 10$). The main difference between the cases $\lambda = 1$ and $\lambda = 5$ is that for $\lambda = 1$ the vesicle inclination angle is significantly larger than that corresponding to $\lambda = 5$.

We investigated the platelet margination for the three values of λ . Figure 4 illustrates more clearly the dependence of the margination phenomenon on λ . It is seen that margination is quite ample for $\lambda = 1$, as compared to the cases $\lambda = 5, 10$. Notably, the distributions of platelets for $\lambda = 5$ and

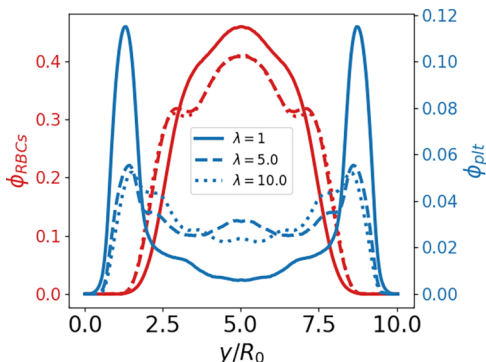


FIG. 4. Time-averaged concentration profile of platelets and RBCs for $\lambda = 1, 5, 10$, $Ca = 30$, $C_n = 0.2$, $\phi = 0.20$, and $\bar{\varepsilon} = 0$. The dashed and solid blue and red lines present the time-averaged concentration profile of platelets and RBCs for $\lambda = 1$ and $\lambda = 10$, respectively.

$\lambda = 10$ are quite close to each other despite the fact for $\lambda = 5$ the vesicle exhibits TT whereas for $\lambda = 10$ it undergoes TB. In conclusion, the margination effect is not associated to TT or TB, but is rather dictated by the importance of lift. As mentioned above, for both $\lambda = 5$ and 10 the lift is small, but in the first case it is due to the small orientation angle of the vesicle with the flow direction (leading to a weak upstream-downstream asymmetry), whereas in the second case it is due to the fact that in the TB regime (and over one TB period) the upstream-downstream asymmetry is very weak (implying a small lift). Note that the platelet concentration increases in the RBC core region for $\lambda = 5, 10$, as shown in Fig. 4. This is attributed to a decrease of lift force, which results in a decrease of CFL, leaving thus more space in the core region where platelets can be trapped. This implies that platelet margination is reduced.

C. The effect of the adhesion energy between red blood cells on platelet margination

In vivo, fibrinogen is believed to be the main actor for adhesion between RBCs. In the case of diabetes, pregnancy, and cardiac diseases, the concentration of fibrinogen is higher than the usual physiological concentration [25], which should enhance the aggregation process [40,60]. In this section we analyze the effect of the adhesion energy between RBCs on platelets margination.

Figure 5 shows snapshots of RBC and platelet configurations in the absence and in the presence of adhesion energy between RBCs. The snapshots are taken at the early stage of simulation and at the end of the simulation. Simulation time t is scaled by τ_c ($\tau_c = \eta_{ex} R_0^3 / k$), which is the typical time needed for the vesicle to return to its equilibrium shape after cessation of flow.

A close inspection of the platelet concentration profile reveals a nontrivial behavior (see Fig. 6). For varying hematocrit levels, a remarkable feature is that a moderate adhesion energy among RBCs ($\bar{\varepsilon} = 15$, corresponding to the lower range of physiological adhesion energy; see Table I) increases the platelet margination. This increase is quite significant for $\phi = 0.2$ than for higher hematocrits. More precisely, for $\phi = 0.2$, the platelet concentration in the cell free layer is increased by about 20% in the presence of modest adhesion, $\bar{\varepsilon} = 15$, as compared to the free-adhesion case. This increase is, however, smaller for $\phi = 0.3$ and $\phi = 0.4$. We will examine in Sec. IV the behavior in microcirculation where hematocrit is in the range 5–20% [27–30], and we will see that the effect of adhesion energy on margination is even ampler. When the adhesion energy among RBCs is significantly increased, there is a decline in platelet margination (Fig. 6). In summary, the platelet margination is nonmonotonic with respect to the adhesion energy between RBCs. Figure 7 illustrates the time-averaged concentration profile of RBCs for different hematocrit levels, $\phi = 0.20, 0.30, 0.40$. For a modest increase of adhesion energy from $\bar{\varepsilon} = 0$ to $\bar{\varepsilon} = 15$ RBCs tend to accumulate more toward the center (green line in Fig. 7) as compared to the case without adhesion

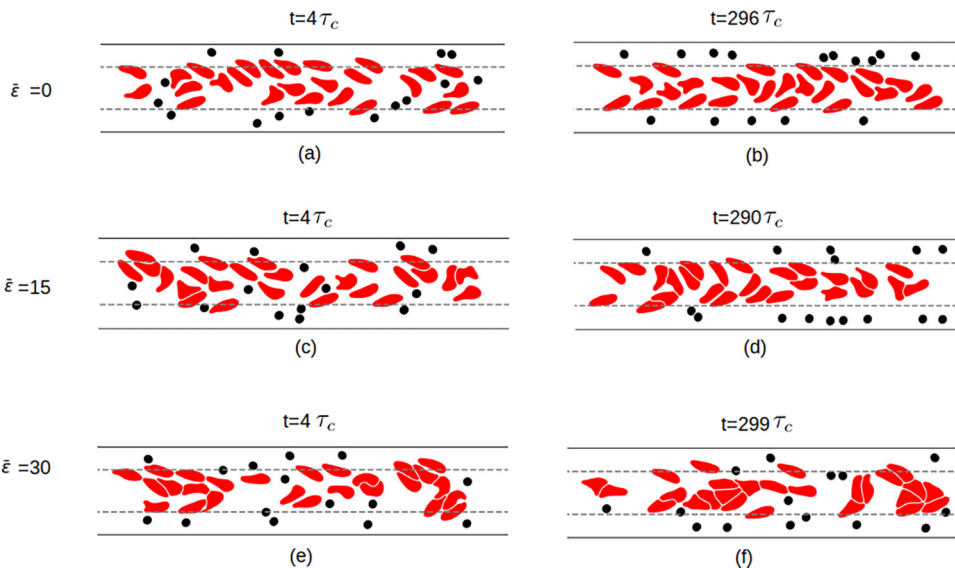


FIG. 5. Snapshots of simulation domain with both RBCs and platelets for different values of adhesion energy between RBCs, $\bar{\epsilon}$. The cell free layer is denoted by horizontal dashed lines.

energy (blue line in Fig. 7). The fact that RBCs accumulate toward the center for a moderate adhesion energy is correlated with the increase of margination discussed above. Increasing further the adhesion energy leads to more accumulation of RBCs toward the periphery. This leads to a decrease of margination. In order to quantify these effects we have calculated the width of the CFL as a function of adhesion energy. Figure 8 confirms the results reported in Fig. 7. There are different ways to define the CFL. Here we follow the method of Ref. [61]. We first calculate the time and space (along x) average concentration profile of RBCs, which depends on y only, $\phi_{\text{RBC}}(y)$. Then we integrate this function over y from zero to a certain y starting from the bottom channel wall and normalize it with the total integrated value over the entire channel width. Then, we define the cell free layer boundary as the location y where only 5% of the total RBC concentration is present from the lower channel wall to that point.

The CFL shows a nonmonotonic behavior (Fig. 8) as a function of the adhesion energy for both hematocrit $\phi = 0.20$ [Fig. 8(a)] and $\phi = 0.40$ [Fig. 8(b)]. This nonmonotonic behavior is correlated with the nonmonotonic platelet margination reported in Fig. 6. The platelet margination mostly occurs after the CFL has fully developed [62]. Platelets are trapped in the CFL during their first

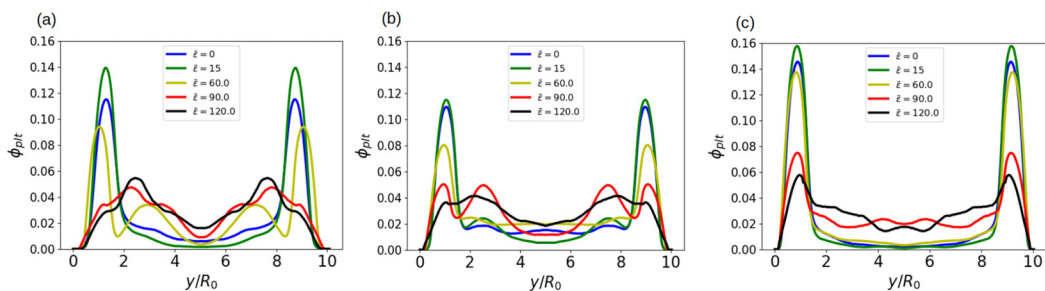


FIG. 6. Time-averaged concentration profile of platelets for (a) $\phi = 0.20$, (b) $\phi = 0.30$, and (c) $\phi = 0.40$. $\bar{\epsilon} = 0, 15, 60, 90, 120$; $\lambda = 1$; $C_n = 0.2$; and $Ca = 30$.

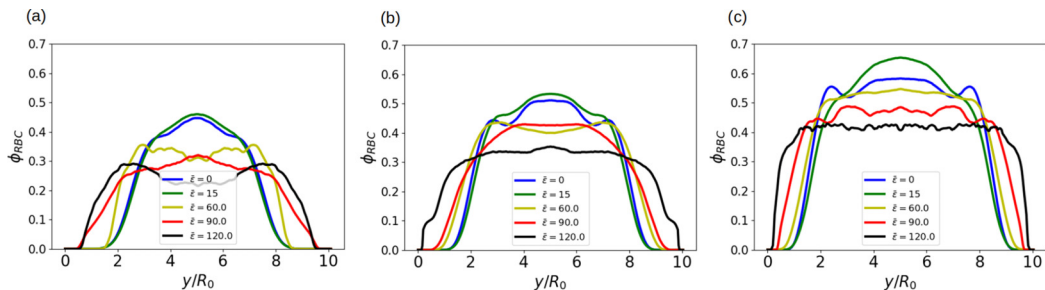


FIG. 7. Time-averaged concentration profile of RBCs for (a) $\phi = 0.20$, (b) $\phi = 0.30$, and (c) $\phi = 0.40$. $\bar{\varepsilon} = 0, 15, 60, 90, 120$; $\lambda = 1$; $C_n = 0.2$; and $Ca = 30$.

visit [20]. For different channel widths we investigated the effect of the adhesion energy between RBCs on cell free layer thickness (Fig. 8). For hematocrit $\phi = 0.20$, capillary number $Ca = 30$, and for different channel widths W , the CFL thickness is found to decrease with increased adhesion energy after an optimum value of $\bar{\varepsilon} = 15$. In addition to the weak number of RBCs undergoing tank treading (which facilitates the transport of platelets into the CFL) in the case of high adhesion energy between RBCs, the CFL thickness is smaller. Therefore, platelets come back to the RBC core before reaching the CFL. According to Figs. 6 and 7, the increase of adhesion energy between RBCs decreases the tendency of platelets to move toward the walls. The increase of RBC aggregation (due to an increase of adhesion energy between RBCs) decreases the number of cells in the middle of the channel as well as the number of free RBCs undergoing tank treading. This section's results validate the previous section's results about the importance of RBC lateral migration for platelet margination.

We have investigated the role of the capillary number on platelet margination, as shown in Fig. 9. It is seen that increasing the capillary number from $Ca = 5$ to $Ca = 70$ notably enhances platelet margination in the presence of adhesion among RBCs. In contrast, when $\bar{\varepsilon} = 0$, the concentration of platelets near the wall is quite insensitive to the capillary number. For both $Ca = 30$ and $Ca = 70$ we observe the nonmonotonic behavior of platelet margination. When Ca is large enough in comparison to unity, most of the cells reach their maximal deformation (saturation due to membrane inextensibility). When Ca is small enough ($Ca = 5$ in the studied case, which corresponds to speed far below those encountered in microcirculation), the lift is small (and so is the CFL), leading

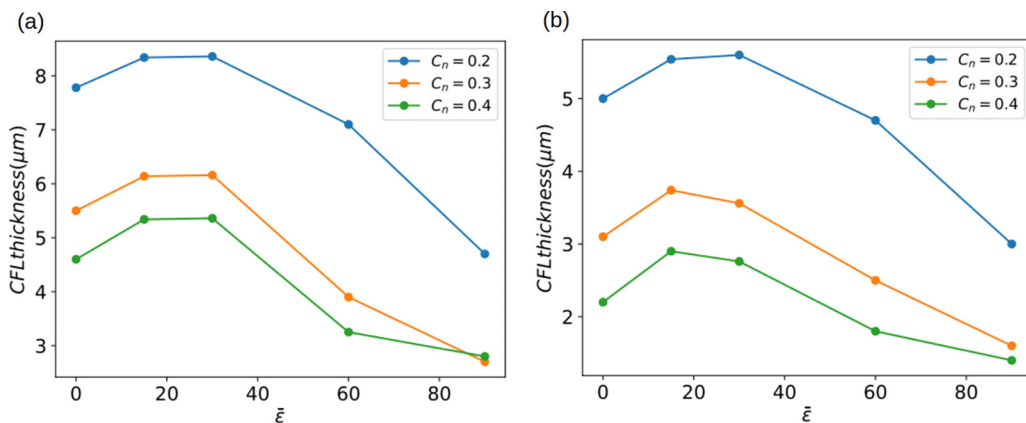


FIG. 8. Cell free layer thickness as a function of adhesion energy $\bar{\varepsilon}$ for all investigated confinement C_n for (a) $\phi = 0.20$ and (b) $\phi = 0.40$.

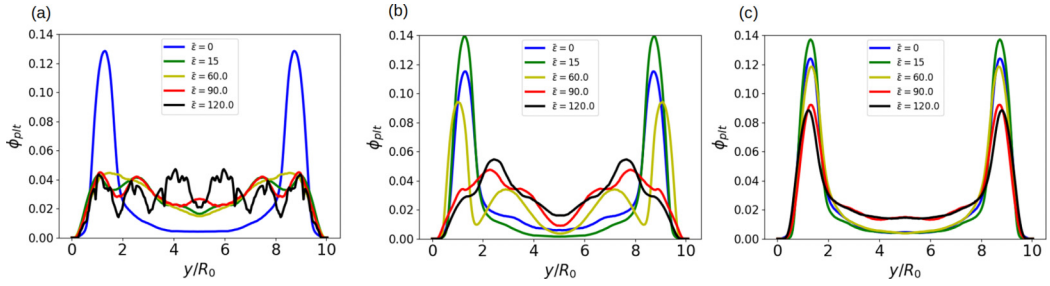


FIG. 9. Time-averaged concentration profile of platelets for (a) $Ca = 5$, (b) $Ca = 30$, and (c) $Ca = 70$. $\bar{\varepsilon} = 0, 15, 60, 90, 120$; $\lambda = 1$; $C_n = 0.2$; and $\phi = 0.20$.

to a moderate margination. In addition, even for a small adhesion energy the aggregate does not significantly break, and provides more space in the core region to trap platelets. Overall, the platelet margination decreases and remains weakly sensitive to an increase of adhesion energy. Finally, Fig. 10 compares platelet trajectories for two values of adhesion energy between RBCs, respectively

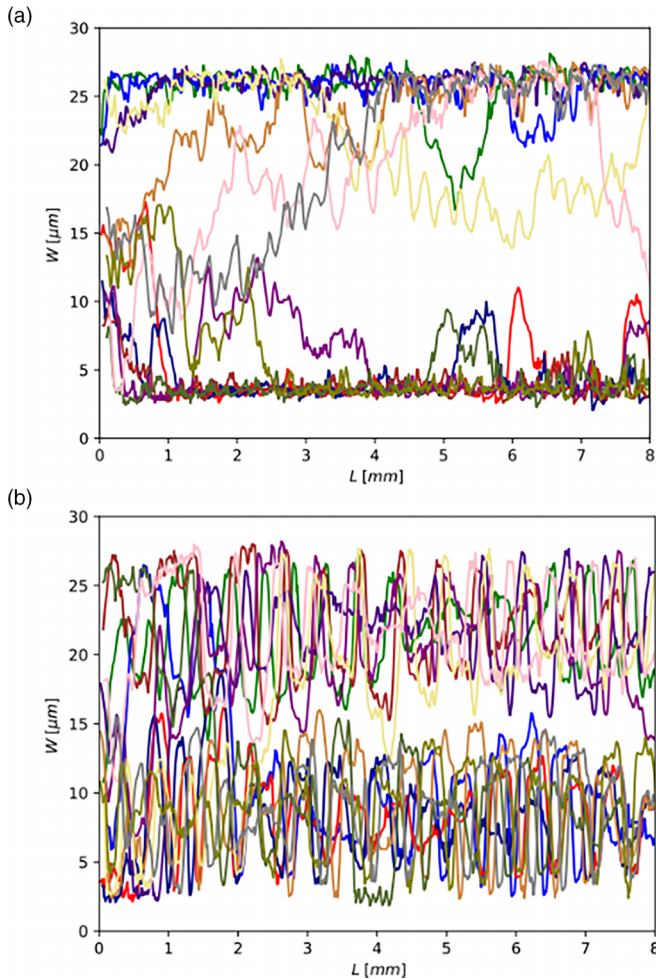


FIG. 10. The platelet trajectories (a) $\bar{\varepsilon} = 0$ and (b) $\bar{\varepsilon} = 90$. $Ca = 30$, $\phi = 0.20$, $\lambda = 1$, and $C_n = 0.2$.

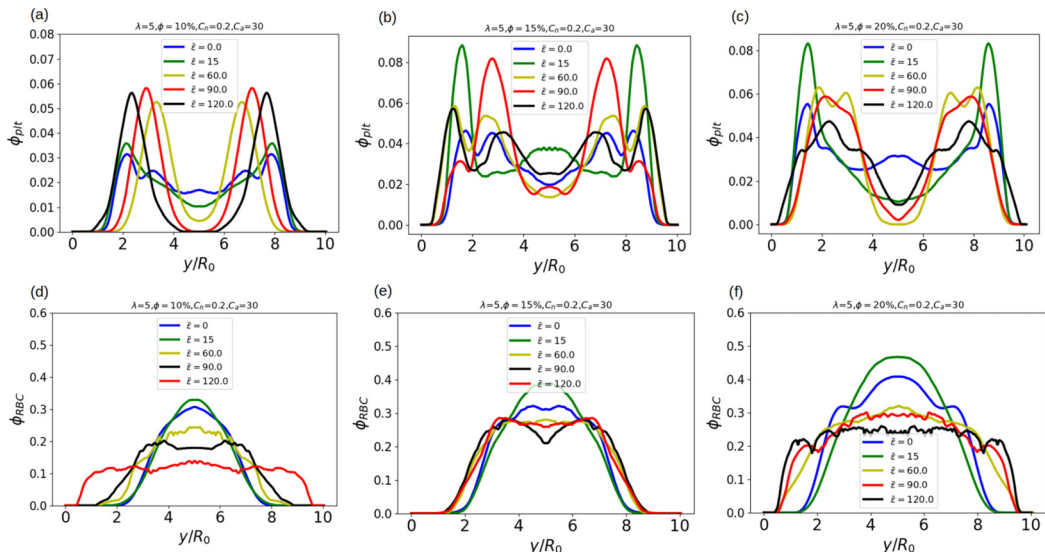


FIG. 11. Top: The platelet profiles. Bottom: RBC profiles for $Ca = 30$, $\lambda = 5$, and for different adhesion energies.

$\bar{\epsilon} = 0$ and $\bar{\epsilon} = 90$. In the absence of adhesion energy, platelets migrate rapidly and the majority reach the outer layer after traveling an average distance of $400 \mu\text{m}$, but, for $\bar{\epsilon} = 90$, platelets stay in the vessel core during their travel through the vessel.

IV. FOCUS ON MICROCIRCULATION WITH A REALISTIC VISCOSITY CONTRAST

In this section we summarize our results relevant for hematocrit in microcirculation, by adopting a viscosity contrast inspired by that of RBCs, namely, $\lambda = 5$. Indeed, in microcirculation hematocrit lies within the 5–20% [27–30] range. We have thus run simulations with $\phi = 0.1, 0.15, 0.2$ and $\lambda = 5$. We have also explored two typical values of flow strength, measured by the capillary number, namely, $Ca = 30$ and $Ca = 70$. Figure 11 shows the platelet profiles and the RBC profiles for $Ca = 30$ for $\phi = 0.1, 0.15, 0.2$ and $\lambda = 5$. Figure 12 shows the results for $Ca = 70$. Both for $Ca = 30$ and $Ca = 70$ we see a nonmonotonic behavior of the platelet profile as a function of adhesion energy. At small and moderate energies the platelet profile peak is boosted by adhesion energy.

A more precise way to show the effect of the adhesion energy on platelet margination is to plot the integrated platelet concentration in the CFL. The result is shown in Fig. 13 for both $Ca = 30$ and $Ca = 70$. In the case of $Ca = 30$, except for $\phi = 0.1$ where the boost is moderate, the impact of adhesion is quite significant for $\phi = 0.15$ and $\phi = 0.2$. In the first case there is about 30% platelet in the CFL in the absence of adhesion, a value that reaches about 50% for adhesion energy $\bar{\epsilon} = 15$. In the second case the platelet proportion in the CFL goes from about 35% in the absence of adhesion to about 58% for $\bar{\epsilon} = 15$. For higher $Ca = 70$ the increase of platelets in CFL is even stronger, going (for $\phi = 0.1$) from 33% (in the absence of adhesion) to 53% for $\bar{\epsilon} = 15$, and (for $\phi = 0.15$) from 30% to about 77% for $\bar{\epsilon} = 90$. These results clearly show an important impact of adhesion energy on platelet margination.

A peculiar behavior is observed for the case of $Ca = 70$ where the platelet concentration in the CFL (Fig. 13) shows a minimum at a certain adhesion energy and increases again at higher adhesion energy. Note that the value of the platelet concentration still remains smaller or close to that in the absence of adhesion energy. To dig further into this effect we focus on the case $\phi = 0.15$ and $Ca = 70$, where the platelet concentration in the CFL reaches a minimum for adhesion energy $\bar{\epsilon} = 90$ and then increases to a relatively larger value at higher adhesion energy $\bar{\epsilon} = 120$ (orange

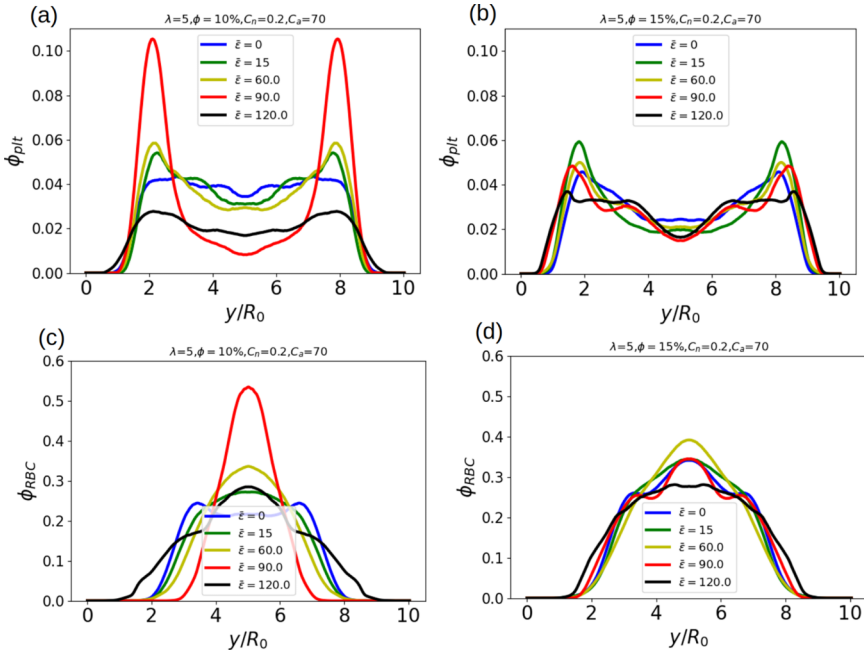


FIG. 12. Top: The platelet profiles. Bottom: RBC profiles for $Ca = 70$, $\lambda = 5$, and for different adhesion energies.

curve in Fig. 13). A snapshot of the cell configuration for each case is represented in Fig. 14. We see there that for $\bar{\epsilon} = 90$ the aggregates are quite rounded with large separation among aggregates, leaving thus ample free space allowing the platelets to explore the central region of the channel. For $\bar{\epsilon} = 120$ larger aggregates form and, due to confinement, the aggregates are more elongated, leaving less free space for platelets to explore the central region. As a consequence due to this geometric configuration the margination is relatively higher for a higher adhesion energy.

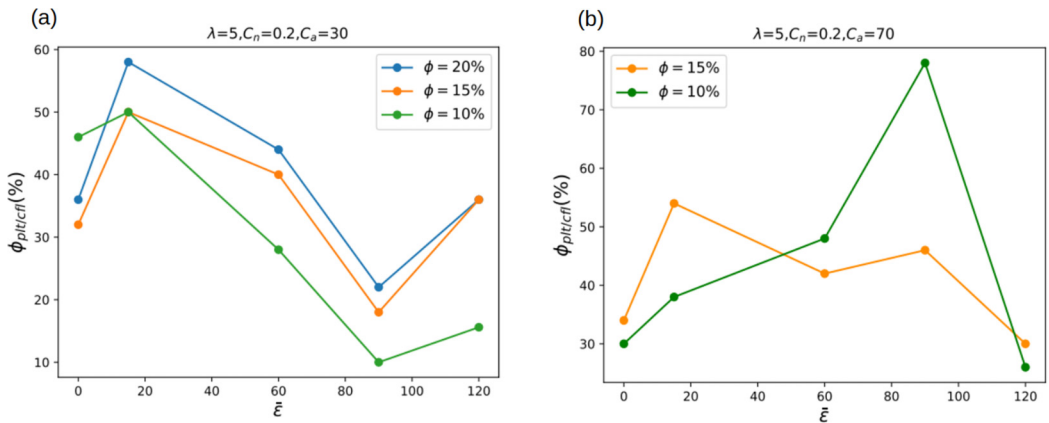


FIG. 13. The integrated platelet profile for (a) $Ca = 30$ and (b) $Ca = 70$, $\lambda = 5$, and different hematocrits as a function of adhesion energy.

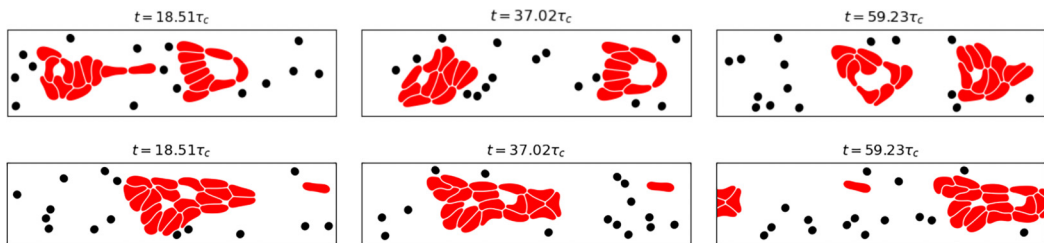


FIG. 14. Snapshots of RBC configuration for $\bar{\epsilon} = 90$ (top) and $\bar{\epsilon} = 120$ (bottom). $\phi = 0.15$, $Ca = 70$, $\lambda = 5$, and $C_n = 0.2$.

V. DISCUSSION

The margination of platelets can be viewed as follows. Suppose we have initially a random distribution of RBCs and platelets within the channel. When the flow is applied, RBCs have a tendency to be pushed away from the walls thanks to the lift mechanism, leaving a CFL close to the walls. At the same time platelets (being rigid) do not experience a significant lift. The platelets which were located initially in the core region will undergo collisions against RBCs and undergo a diffusionlike process (of hydrodynamic origin). This diffusion will cause platelets to spread across streamlines. Once a platelet reaches the CFL it will be trapped there, owing to the absence of a significant lift. This process is efficient for a large enough hematocrit, as reported in Ref. [4].

For a modest adhesion energy (middle panels in Fig. 5) some RBCs, initially at the extreme peripheries, will be weakly attracted by some RBCs sitting in the next files of RBCs, leading to a small fraction of small clusters (while there are many single RBCs), like RBC doublets (see middle panel in Fig. 5). This increases the CFL width. This will naturally enhance the margination process. For a larger adhesion energy (see lower panel in Fig. 5), large enough clusters form. This has two consequences: (i) the clusters often rotate (as described in detail for doublets in Ref. [33]), and as for a tumbling RBC, the lift is reduced, leading to a reduction of the CFL, and (ii) the formation of many clusters in the core region increases free cell spaces, allowing thereby platelets to visit more easily these regions, even for those initially in the CFL, thanks to collision with RBC clusters. These two mechanisms lead to a decline of platelet margination.

There are several diseases which are known to lead to robust aggregation among RBCs. A well-known situation is that encountered in diabetes mellitus [25]. The precise origin of enhanced aggregation for patients suffering diabetes is not yet completely elucidated, albeit the formation of robust clusters of RBCs is beyond any doubt. It is well documented that these patients suffer from uncontrolled bleeding for which several factors have been reported in Ref. [63], such as coagulation disorders, hypofibrinolysis, and changes in platelet number and activation. It will be an important task for future investigations to elucidate if the mechanisms reported here may contribute efficiently to uncontrolled bleeding for diabetic patients. There are, however, several cautions. It has been reported that the channel length must be of the order of $300 \mu\text{m}$ before full platelet margination can take place [6]. Those studies, as well as the present one, pertain to microvascular networks, in which the vessel length rarely exceeds this length, before meeting a bifurcation. Several studies have explored the process of platelets and other blood cells marginating within bifurcations [14,64,65]. Bächer *et al.* [64] showed that a bifurcation does not significantly impact platelet margination, provided that the initial configuration corresponds to platelets which are close to the channel walls in the mother branch. In contrast, a confluence is found to reduce the margination [64]. Noguchi *et al.* [65] reported that a distance of 5 mm is necessary after a confluence for platelets to marginate again [65]. It is important to study the margination process in a realistic network (containing bifurcations and confluences) where platelets are initially randomly positioned in a mother vessel, and analyze the influence of various parameters (flow strength, hematocrit, RBC aggregation, viscosity contrast) that could affect platelet behavior.

VI. CONCLUSION

We have investigated the platelet margination in a simple straight channel in the presence of adhesion energy among RBCs. We have first clarified the role of the lift in the process of margination, by showing that even if RBCs undergo tank-treading (TT) behavior the platelet margination can be as weak as in the case when they exhibit tumbling. If the orientation angle of the RBCs is weak enough the effect of margination can be as weak as in the case for a tumbling (TB) cell. This is attributed to the weak upstream-downstream asymmetry, and not to the fact that a cell is in the TT or TB regime. We have then investigated the role of adhesion in the process of margination. A remarkable feature discovered here is that the margination is nonmonotonic with respect to the adhesion energy. A modest adhesion energy, as encountered under normal physiological conditions, is found to boost the margination process, whereas a strong enough adhesion leads to a decline of margination. We have provided an intuitive explanation for this behavior. As highlighted in the previous section, the typical channel length for a complete margination of platelets is several hundreds of micrometers, a length which generally exceeds that of vessels in microvascular networks. In order to have a complete picture of margination *in vivo* a simulation in a realistic vascular network is necessary. Finally, our simulation has a limitation since it is based on two dimensions, which serves at least as a guide. While it has been shown in different works that the 2D model captures several features observed in three dimensions [31–37], a full three-dimensional simulation is necessary before drawing definite conclusive answers. It is hoped to investigate this matter further in a future work.

ACKNOWLEDGMENTS

We acknowledge financial support from CNES (Centre National d'Etudes Spatiales), and the French-German University Programme "Living Fluids" (Grant No. CFDA-Q1-14). M.D. and C.M. acknowledge funding by the Marie Skłodowska-Curie Grant Agreement No. 860436, EVIDENCE. The simulations were performed on the Cactus cluster of the CIMENT infrastructure, which is supported by the Rhône-Alpes region (Grant No. CPER07_13 CIRA).

-
- [1] J. N. Thon and J. E. Italiano, Platelets: Production, morphology and ultrastructure, in *Antiplatelet Agents* (Springer, Berlin, 2012), pp. 3–22.
 - [2] V. W. M. van Hinsbergh, Endothelium—role in regulation of coagulation and inflammation, in *Seminars in Immunopathology* (Springer, Berlin, 2012), Vol. 34, pp. 93–106.
 - [3] J. S. Pober and W. C. Sessa, Evolving functions of endothelial cells in inflammation, *Nat. Rev. Immunol.* **7**, 803 (2007).
 - [4] T. Krüger, Effect of tube diameter and capillary number on platelet margination and near-wall dynamics, *Rheol. Acta* **55**, 511 (2016).
 - [5] H.-Y. Chang, A. Yazdani, X. Li, K. A. A. Douglas, C. S. Mantzoros, and G. E. Karniadakis, Quantifying platelet margination in diabetic blood flow, *Biophys. J.* **115**, 1371 (2018).
 - [6] D. A. Reasor, M. Mehrabadi, D. N. Ku, and C. K. Aidun, Determination of critical parameters in platelet margination, *Ann. Biomed. Eng.* **41**, 238 (2013).
 - [7] A. W. Tilles and E. C. Eckstein, The near-wall excess of platelet-sized particles in blood flow: Its dependence on hematocrit and wall shear rate, *Microvasc. Res.* **33**, 211 (1987).
 - [8] A. E. Moskalensky, M. A. Yurkin, A. R. Muliukov, A. L. Litvinenko, V. M. Nekrasov, A. V. Chernyshev, and V. P. Maltsev, Method for the simulation of blood platelet shape and its evolution during activation, *PLoS Comput. Biol.* **14**, e1005899 (2018).
 - [9] L. Li, S. Wang, K. Han, X. Qi, S. Ma, L. Li, J. Yin, D. Li, X. Li, and J. Qian, Quantifying shear-induced margination and adhesion of platelets in microvascular blood flow, *J. Mol. Biol.* **435**, 167824 (2023).

- [10] D. A. Fedosov, J. Fornleitner, and G. Gompper, Margination of white blood cells in microcapillary flow, *Phys. Rev. Lett.* **108**, 028104 (2012).
- [11] D. A. Fedosov and G. Gompper, White blood cell margination in microcirculation, *Soft Matter* **10**, 2961 (2014).
- [12] H. L. Goldsmith and S. Spain, Margination of leukocytes in blood flow through small tubes, *Microvasc. Res.* **27**, 204 (1984).
- [13] W. Marth, S. Aland, and A. Voigt, Margination of white blood cells: A computational approach by a hydrodynamic phase field model, *J. Fluid Mech.* **790**, 389 (2016).
- [14] B. Namgung, Y. C. Ng, H. L. Leo, J. M. Rifkind, and S. Kim, Near-wall migration dynamics of erythrocytes in vivo: Effects of cell deformability and arteriolar bifurcation, *Front. Physiol.* **8**, 963 (2017).
- [15] C. Bächer, L. Schrack, and S. Gekle, Clustering of microscopic particles in constricted blood flow, *Phys. Rev. Fluids* **2**, 013102 (2017).
- [16] D. Oh, S. Ii, and S. Takagi, Numerical study of particle margination in a square channel flow with red blood cells, *Fluids* **7**, 96 (2022).
- [17] Q. M. Qi and E. S. G. Shaqfeh, Theory to predict particle migration and margination in the pressure-driven channel flow of blood, *Phys. Rev. Fluids* **2**, 093102 (2017).
- [18] Q. M. Qi and E. S. G. Shaqfeh, Time-dependent particle migration and margination in the pressure-driven channel flow of blood, *Phys. Rev. Fluids* **3**, 034302 (2018).
- [19] A. Yazdani, Y. Deng, H. Li, E. Javadi, Z. Li, S. Jamali, C. Lin, J. D. Humphrey, C. S. Mantzoros, and G. E. Karniadakis, Integrating blood cell mechanics, platelet adhesive dynamics and coagulation cascade for modelling thrombus formation in normal and diabetic blood, *J. R. Soc. Interface* **18**, 20200834 (2021).
- [20] H. Zhao and E. S. G. Shaqfeh, Shear-induced platelet margination in a microchannel, *Phys. Rev. E* **83**, 061924 (2011).
- [21] P. A. Aarts, S. A. Van Den Broek, G. W. Prins, G. D. Kuiken, J. J. Sixma, and R. M. Heethaar, Blood platelets are concentrated near the wall and red blood cells, in the center in flowing blood, *Arteriosclerosis* **8**, 819 (1988).
- [22] G. Coutinho, A. S. Moita, M. Rossi, and A. L. N. Moreira, Experimental perspective on the mechanisms for near-wall accumulation of platelet-size particles in pressure-driven red blood cell suspension flows, *Phys. Rev. Fluids* **8**, 103101 (2023).
- [23] B. Czaja, M. Gutierrez, G. Závodszky, D. de Kanter, A. Hoekstra, and O. Eniola-Adefeso, The influence of red blood cell deformability on hematocrit profiles and platelet margination, *PLoS Comput. Biol.* **16**, e1007716 (2020).
- [24] A. P. Spann, J. E. Campbell, S. R. Fitzgibbon, A. Rodriguez, A. P. Cap, L. H. Blackburne, and E. S. G. Shaqfeh, The effect of hematocrit on platelet adhesion: Experiments and simulations, *Biophys. J.* **111**, 577 (2016).
- [25] P. Foresto, M. D'Arrigo, L. Carreras, R. E. Cuzzo, J. Valverde, and R. Rasia, Evaluation of red blood cell aggregation in diabetes by computerized image analysis, *Medicina (Buenos Aires, Argent.)* **60**, 570 (2000).
- [26] R. Barazzoni, M. Zanetti, G. Davanzo, E. Kiwanuka, P. Carraro, A. Tiengo, and P. Tessari, Increased fibrinogen production in type 2 diabetic patients without detectable vascular complications: Correlation with plasma glucagon concentrations, *J. Clin. Endocrinol. Metab.* **85**, 3121 (2000).
- [27] J. Boyle III, Microcirculatory hematocrit and blood flow, *J. Theor. Biol.* **131**, 223 (1988).
- [28] B. Klitzman and B. R. Duling, Microvascular hematocrit and red cell flow in resting and contracting striated muscle, *Am. J. Physiol.* **237**, H481 (1979).
- [29] G. Li, T. Ye, Z. Xia, S. Wang, and Z. Zhu, Analysis and prediction of hematocrit in microvascular networks, *Int. J. Eng. Sci.* **191**, 103901 (2023).
- [30] H. H. Lipowsky, S. Usami, and S. Chien, In vivo measurements of "apparent viscosity" and microvessel hematocrit in the mesentery of the cat, *Microvasc. Res.* **19**, 297 (1980).
- [31] B. Kaoui, N. Tahiri, T. Biben, H. Ez-Zahraouy, A. Benyoussef, G. Biros, and C. Misbah, Complexity of vesicle microcirculation, *Phys. Rev. E* **84**, 041906 (2011).
- [32] B. Kaoui, G. Biros, and C. Misbah, Why do red blood cells have asymmetric shapes even in a symmetric flow? *Phys. Rev. Lett.* **103**, 188101 (2009).

- [33] M. Abbasi, A. Farutin, A. Nait-Ouhra, H. Ez-Zahraouy, A. Benyoussef, and C. Misbah, Dynamics and rheology of a single two-dimensional multilobe vesicle in a confined geometry, *Phys. Rev. Fluids* **7**, 093603 (2022).
- [34] L. Lanotte, J. Mauer, S. Mendez, D. A. Fedosov, J.-M. Fromental, V. Claveria, F. Nicoud, G. Gompper, and M. Abkarian, Red cells' dynamic morphologies govern blood shear thinning under microcirculatory flow conditions, *Proc. Natl. Acad. Sci. USA* **113**, 13289 (2016).
- [35] J. Mauer, S. Mendez, L. Lanotte, F. Nicoud, M. Abkarian, G. Gompper, and D. A. Fedosov, Flow-induced transitions of red blood cell shapes under shear, *Phys. Rev. Lett.* **121**, 118103 (2018).
- [36] D. Flormann, O. Aouane, L. Kaestner, C. Ruloff, C. Misbah, T. Podgorski, and C. Wagner, The buckling instability of aggregating red blood cells, *Sci. Rep.* **7**, 7928 (2017).
- [37] M. Abbasi, A. Farutin, H. Ez-Zahraouy, A. Benyoussef, and C. Misbah, Erythrocyte-erythrocyte aggregation dynamics under shear flow, *Phys. Rev. Fluids* **6**, 023602 (2021).
- [38] O.-Y. Zhong-can and W. Helfrich, Bending energy of vesicle membranes: General expressions for the first, second, and third variation of the shape energy and applications to spheres and cylinders, *Phys. Rev. A* **39**, 5280 (1989).
- [39] S. Chien and Kung-ming Jan, Ultrastructural basis of the mechanism of rouleaux formation, *Microvasc. Res.* **5**, 155 (1973).
- [40] M. Brust, O. Aouane, M. Thiébaud, D. Flormann, C. Verdier, L. Kaestner, M. W. Laschke, H. Selmi, A. Benyoussef, and T. Podgorski, The plasma protein fibrinogen stabilizes clusters of red blood cells in microcapillary flows, *Sci. Rep.* **4**, 4348 (2014).
- [41] V. Claveria, O. Aouane, M. Thiébaud, M. Abkarian, G. Coupier, C. Misbah, T. John, and C. Wagner, Clusters of red blood cells in microcapillary flow: Hydrodynamic versus macromolecule induced interaction, *Soft Matter* **12**, 8235 (2016).
- [42] B. Neu and H. J. Meiselman, Depletion-mediated red blood cell aggregation in polymer solutions, *Biophys. J.* **83**, 2482 (2002).
- [43] K. Buxbaum, E. Evans, and D. E. Brooks, Quantitation of surface affinities of red blood cells in dextran solutions and plasma, *Biochemistry* **21**, 3235 (1982).
- [44] Y. Liu and W. K. Liu, Rheology of red blood cell aggregation by computer simulation, *J. Comput. Phys.* **220**, 139 (2006).
- [45] T. C. Lim, The relationship between Lennard-Jones (12-6) and Morse potential functions, *Z. Naturforsch. A* **58**, 615 (2003).
- [46] P. Steffen, C. Verdier, and C. Wagner, Quantification of depletion-induced adhesion of red blood cells, *Phys. Rev. Lett.* **110**, 018102 (2013).
- [47] B. Kaoui, G. H. Ristow, I. Cantat, C. Misbah, and W. Zimmermann, Lateral migration of a two-dimensional vesicle in unbounded poiseuille flow, *Phys. Rev. E* **77**, 021903 (2008).
- [48] C. S. Peskin, The immersed boundary method, *Acta Numer.* **11**, 479 (2002).
- [49] Z. Shen, A. Farutin, M. Thiébaud, and C. Misbah, Interaction and rheology of vesicle suspensions in confined shear flow, *Phys. Rev. Fluids* **2**, 103101 (2017).
- [50] B. Kaoui and J. Harting, Two-dimensional lattice Boltzmann simulations of vesicles with viscosity contrast, *Rheol. Acta* **55**, 465 (2016).
- [51] B. Kaoui, J. Harting, and C. Misbah, Two-dimensional vesicle dynamics under shear flow: Effect of confinement, *Phys. Rev. E* **83**, 066319 (2011).
- [52] T. Krüger, F. Varnik, and D. Raabe, Efficient and accurate simulations of deformable particles immersed in a fluid using a combined immersed boundary lattice Boltzmann finite element method, *Comput. Math. Appl.* **61**, 3485 (2011).
- [53] T. Krüger, S. Frijters, F. Günther, B. Kaoui, and J. Harting, Numerical simulations of complex fluid-fluid interface dynamics, *Eur. Phys. J.: Spec. Top.* **222**, 177 (2013).
- [54] N. Takeishi, M. E. Rosti, Y. Imai, S. Wada, and L. Brandt, Haemorheology in dilute, semi-dilute and dense suspensions of red blood cells, *J. Fluid Mech.* **872**, 818 (2019).
- [55] L. Bureau, G. Coupier, and T. Salez, Lift at low Reynolds number, *Eur. Phys. J. E* **46**, 111 (2023).
- [56] S. Nix, Y. Imai, and T. Ishikawa, Lateral migration of a capsule in a parabolic flow, *J. Biomech.* **49**, 2249 (2016).

- [57] B. Kaoui, A. Farutin, and C. Misbah, Vesicles under simple shear flow: Elucidating the role of relevant control parameters, *Phys. Rev. E* **80**, 061905 (2009).
- [58] B. Kaoui, R. J. W. Jonk, and J. Harting, Interplay between microdynamics and macrorheology in vesicle suspensions, *Soft Matter* **10**, 4735 (2014).
- [59] A. Nait-Ouhra, A. Farutin, H. Ez-Zahraouy, A. Benyoussef, and C. Misbah, Rheology of a confined vesicle suspension, *Phys. Rev. Fluids* **4**, 103602 (2019).
- [60] A. Maslianitsyna, P. Ermolinskiy, A. Lugovtsov, A. Pigurenko, M. Sasonko, Y. Gurfinkel, and A. Priezhev, Multimodal diagnostics of microrheologic alterations in blood of coronary heart disease and diabetic patients, *Diagnostics* **11**, 76 (2021).
- [61] X. Yin, T. Thomas, and J. Zhang, Multiple red blood cell flows through microvascular bifurcations: Cell free layer, cell trajectory, and hematocrit separation, *Microvasc. Res.* **89**, 47 (2013).
- [62] L. M. Crowl and A. L. Fogelson, Computational model of whole blood exhibiting lateral platelet motion induced by red blood cells, *Int. J. Numer. Methods Biomed. Eng.* **26**, 471 (2010).
- [63] X. Li, N. C. Weber, D. M. Cohn, M. W. Hollmann, J. H. DeVries, J. Hermanides, and B. Preckel, Effects of hyperglycemia and diabetes mellitus on coagulation and hemostasis, *J. Clin. Med.* **10**, 2419 (2021).
- [64] C. Bächer, A. Kihm, L. Schrack, L. Kaestner, M. W. Laschke, C. Wagner, and S. Gekle, Antimargination of microparticles and platelets in the vicinity of branching vessels, *Biophys. J.* **115**, 411 (2018).
- [65] A. Noguchi, Y. Tange, T. Itano, and M. Sugihara-Seki, Margination of platelet-sized particles in red blood cell suspensions flowing through a Y-shaped confluence microchannel, *Fluid Dyn. Res.* **55**, 035506 (2023).